Exploring the Impact of Active Site Structure on the Conversion of Methane to Methanol in Cu-Exchanged Zeolites

Florian Göltl^{1,2,*}, Saurabh Bhandari², Edgard A. Lebrón-Rodríguez², Jake I. Gold², Daniel J. Hutton¹, Stacey I. Zones³, Ive Hermans^{2,4}, James A. Dumesic², Manos Mavrikakis^{2,*}

¹ The University of Arizona, Department of Biosystems Engineering, 1177, E 4th St., 85719, Tucson, AZ, United States

²The University of Wisconsin – Madison, Department of Chemical and Biological Engineering, 1415 Engineering Drive, 53706 Madison, WI, United States

³ Chevron Energy Technology Company, Richmond, CA, 94804, United States

⁴ The University of Wisconsin – Madison, Department of Chemistry, 1101 University Avenue, 53706 Madison, WI, United States

email: fgoeltl@arizona.edu; emavrikakis@wisc.edu

Abstract:

In the past, Cu-oxo or -hydroxy clusters hosted in zeolites have been suggested to enable the selective conversion of methane to methanol, but the impact of the active site's stoichiometry and structure on methanol production is still poorly understood. Herein, we apply theoretical modeling in conjunction with experiments to study the impact of these two factors on partial methane oxidation in the Cu-exchanged zeolite SSZ-13. Phase diagrams developed from first-principles suggest that Cu-hydroxy or Cu-oxo dimers are stabilized when O2 or N2O are used to activate the catalyst, respectively. We confirm these predictions experimentally and determine that in a stepwise conversion process, Cu-oxo dimers can convert twice as much methane to methanol compared to Cu-hydroxyl dimers. Our theoretical models rationalize how Cu-di-oxo dimers can convert up to two methane molecules to methanol, while Cu-di-hydroxyl dimers can convert only one methane molecule to methanol per catalytic cycle. These findings imply that in Cu clusters, at least one oxo group or two hydroxyl groups are needed to convert one methane molecule to methanol per cycle. This simple structure-activity relationship allows to intuitively understand the potential of small oxygenated or hydroxylated transition metal clusters to convert methane to methanol.

Introduction:

Methane, the main component of natural gas, is a greenhouse agent, which is up to 85 times more potent than CO₂. Its transport requires elaborate infrastructure, and it is difficult to convert to higher value products. For these reasons, natural gas is an undesirable byproduct in the extraction of oil in remote locations and is in many cases flared at the extraction site. Flaring of natural gas is a significant contributor to global CO₂ emissions. Accordingly, the selective conversion of methane to higher-value and easier-to-transport chemicals is highly desirable. Currently, industry converts methane using an indirect route, whereby methane is first converted into synthesis gas, which is then catalytically transformed into long-chain hydrocarbons¹, higher alcohols², or methanol³. However, this process requires high pressures and temperatures and is feasible only at a large scale. Thus, a direct route for the conversion of methane to higher-value chemicals that can be practiced in remote locations and at smaller scales would be very valuable.

Breaking the first C-H bond in methane is more difficult than the activation of subsequent C-H bonds, imposing an inherent selectivity challenge. As a result, most catalysts do not stop methane's conversion at methanol but causes over-oxidizing to CO₂⁴. One class of materials that can selectively convert methane to methanol is metal-exchanged zeolites, ^{5–12} and in particular Cu-exchanged zeolites have attracted attention. After activation at high temperature in an oxidative environment, Cu-oxo^{13,14,23,24,15–22} and Cu-hydroxy clusters, ^{25,26} active in the conversion of methane, are stabilized in these zeolites. Although the catalytic conversion of methane with low conversion²⁷ rates or low selectivities²⁸ to methanol has been reported, the reaction is most often pursued in a stepwise process²⁵.

Despite intense research efforts in this area, the exact nature of the active sites in Cu-exchanged zeolites is still under debate. Many different site structures and stoichiometries, ranging from Cu-oxo dimers^{13,15,18,29–31} and trimers¹⁷, Cu-hydroxy dimers^{21,25,26,32}, single or paired Cu-hydroxy monomers^{33–35}, or even Cu-oxo dimers stabilized by extraframework Al species^{36,37}, have been proposed to be present in different zeolite structures. This uncertainty has led to the notion that many different Cu-oxo or Cu-hydroxy sites might be present in Cu-exchanged zeolites, and that many of them are able to convert methane to methanol⁵. However, a detailed understanding of the impact of active site structure on methane conversion to methanol is still lacking.

In this contribution, we combine first-principles modeling with experimental measurements to explore the impact of active site structure on the conversion of methane to methanol over Cu-exchanged SSZ-13. Following previously-developed design principles for zeolite catlaysts^{38,39}, we use phase diagrams developed from first-principles to design experimental measurements at conditions where Cu-hydroxy dimers and Cu-oxo dimers are stabilized. We confirm the presence of the desired sites using UV-vis-NIR and Raman spectroscopy. Lastly, we explore the impact of site structure on methane conversion by combining activity measurements and theoretical modeling of the respective reaction pathways.

Results:

Phase Diagrams: The conversion of methane to methanol over zeolites usually follows a stepwise process:^{25,40} (i) the zeolite is initially exposed to an oxidizing agent at high temperatures (e.g., 723 K); (ii) the system is cooled to lower temperatures (e.g., 473 K) and exposed to methane; and (iii) methanol is extracted. The duration of each step is on the order of hours⁴⁰, and therefore, given the mobility of Cu ions in zeolites⁴¹, we assume that the system is thermodynamically equilibrated at the end of each step. For such an operation protocol, phase diagrams are an ideal tool to explore the nature of the Cu sites after activation. Here, the chemical potential of Cu in different bonding environments is compared to identify the thermodynamically most stable structure over a wide range of conditions^{25,39}. In the following, we will focus on SSZ-13, a small pore zeolite that, due to its small primitive unit cell, is an ideal zeolite model system.⁴² Its Cu-exchanged form is an industrially applied redox catalyst,^{41,43-45} and it has been extensively studied in the conversion of methane to methanol.^{13,15,18,21,25,26} In a previous study, we developed phase diagrams for Cu-SSZ-13 activated in an O₂ atmosphere, and we will use this model as a basis for our current analysis.²⁵

SSZ-13 is a zeolite in the chabazite structure with a primitive unit cell that contains only 12 T-sites (T stands for either Si or Al) and 24 O atoms (see Figure 1). Siliceous zeolites, i.e., zeolites that contain only Si but no Al, are chemically inert, but the framework can be chemically activated by the presence of Al. In protonated zeolites, a proton is associated with each Al atom, but using ion exchange, Cu can be introduced to the system and replaces H atoms. The difficulty in constructing phase diagrams is connected to the fact that, in a realistic zeolite, a distribution of Al atoms is present. These Al atoms serve as anchoring points for Cu sites, and depending on the relative position of the Al atoms, different exchange positions exist in the framework.^{25,46–48} Here, we use a model for medium to high Si/Al ratio zeolites (Si/Al>8), which includes six different Al configurations with either one or two Al atoms per unit cell for Cu monomers (2Al-A through 2Al-E, 1Al) and four different Al configurations for Cu dimers and trimers (D-A through D-D, see Figure 1). For Cu monomers, we consider Cu(I), Cu associated with 1 Al atom and formally in a +1 oxidation state, and Cu(II), Cu associated with two Al atoms and formally in a +2 oxidation state, bonded with up to six water molecules as well as Cu-OH bonded with up to five water molecules⁴⁹. For the dimer/trimer exchange sites, we study all different Cu₂O_vH_z structures with $1 \le y \le 2$ and $0 \le z \le y$ and $Cu_3O_3H_z$ with $0 \le z \le 3^{25}$. We do not consider any larger Cu structures since, to the best of our knowledge, they have not been observed experimentally. This leads to a total of 36 dimer/trimer structures and 125 monomer structures. Henceforth, Cu_xO_vH_z in dimer anchoring configuration D-X (X = A, B, C, or D) will be labeled as $X-Cu_xO_vH_z$. Structures and preferred spin states for Cu trimers in the D-C and D-D exchange position are given in the Supporting Information, section S2 and structure files are provided in the supporting structures file. All other structures and their respective spin states have been previously published in the literature^{25,49}, and a graphical representation of all dimers and trimers studied is given in Figure S3 in the Supporting Information. To take the finite number of Cu atoms in the zeolite matrix after ion exchange into account, we do not include a metallic or metal-oxide reference state for Cu in our phase diagrams. Accordingly, we will display phase diagrams that include all four dimer anchoring configurations and one monomer anchoring configuration. These phase diagrams allow the identification of the overall most stable sites. However, in a realistic zeolite, a distribution of Al configurations is present,⁴⁴ which is determined by materials synthesis⁵⁰. To identify the Cu sites present for each part of the distribution of Al configurations, phase diagrams for all combinations of one dimer exchange configuration and one monomer exchange configuration are therefore shown in the Supporting Information, Figures S4 and S5. A detailed legend to phase diagrams is given in Figure S14 in the Supporting Information and more details regarding this model are given in the literature.²⁵

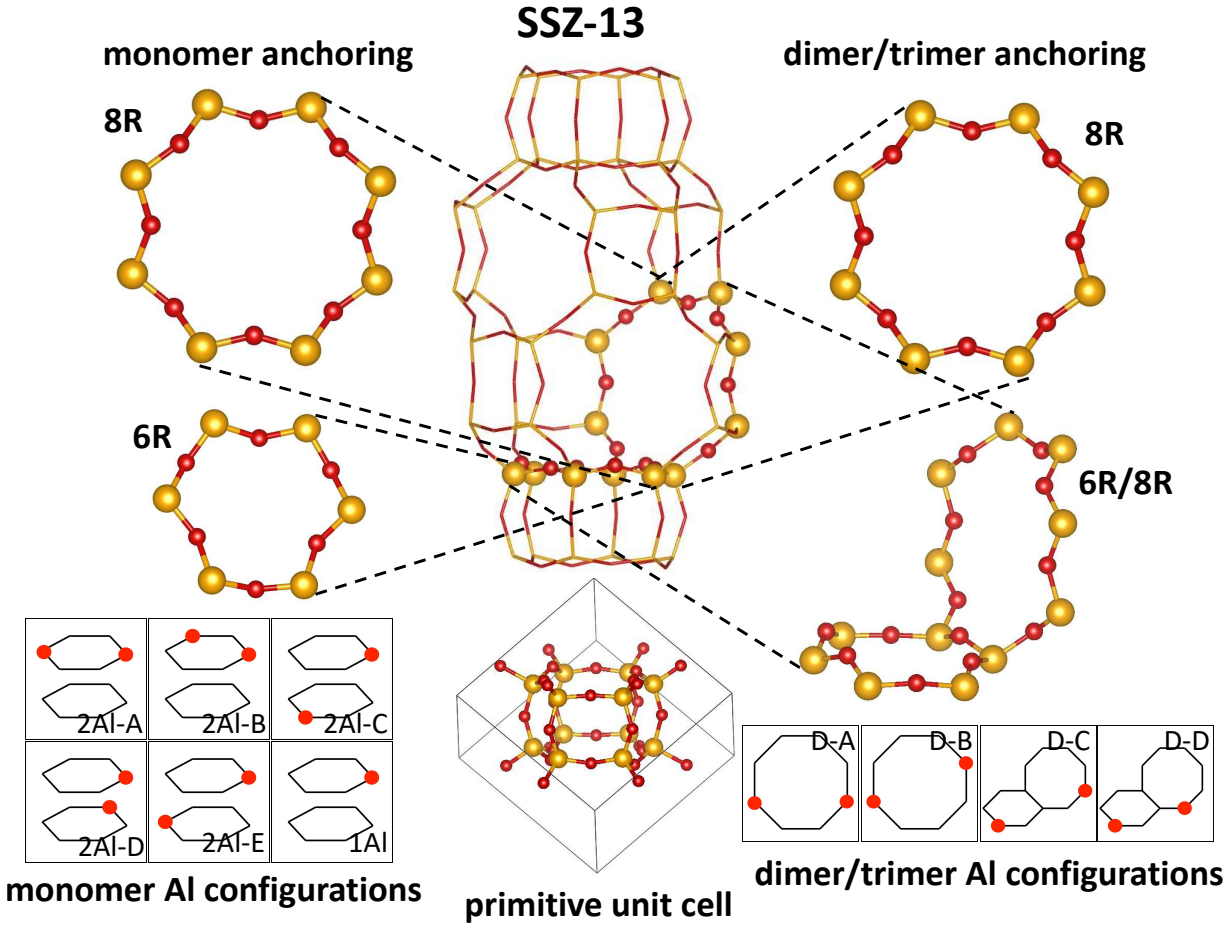


Figure 1: Atomistic representation of the main cage of SSZ-13. In the center, the main cage with adjacent double six-ring units, as well as the primitive unit cell is displayed. On the left, different Cu monomer exchange positions in the six ring (6R) and eight ring (8R) and Al configurations for Cu monomer anchoring are displayed. On the right, different exchange positions in the eight ring (8R, D-A, and D-B) and bridging the six ring and eight ring (6R/8R, D-C and D-D) and Al anchoring configurations for Cu dimers and trimers studied in this work are shown. In atomistic images, yellow atoms correspond to Si and red atoms to O, respectively. Ring structures for ion exchange are represented in a ball and stick model, while the remainder of the cage is displayed in a stick representation. Dashed lines are used to highlight the position of exchange sites with respect to the main cage. In schematic representations, black lines correspond to a Si(Al)-O-Si link, Si atoms are positioned at the vertices, and red circles indicate the position of the Al atoms.

In the past, different Cu monomers^{46,47,49,51,52} and dimers^{13,15,18,21,25} have been suggested to be present in Cu-SSZ-13. As a first step, we ask the question: which Cu sites can theoretically be stabilized in this material as a function of experimental conditions? To achieve this goal, we focus on phase diagrams where the chemical potential of Cu in a Cu site with stoichiometry $Cu_xO_yH_z$ ($\mu^{Cu}_{Cu_xO_yH_z}$) is calculated with respect to the abstract quantities μ_H and μ_O , the chemical potential of hydrogen and oxygen, respectively. These phase diagrams reveal that Cu_2O , Cu_2O_2 , Cu_2OH , and $Cu_2O_2H_2$ can be stabilized in SSZ-13. At the same time, we find, that in SSZ-13 trimers will not be

stabilized under any conditions. A detailed discussion and all phase diagrams are provided in Section S3.2 of the Supporting Information.

To translate the abstract quantities μ_H and μ_O to realistic gas phase conditions related to experiments, we explored two different sets of conditions, namely, activation in: (1) O2 atmosphere and (2) N₂O atmosphere. The mathematical expressions of $\mu_{Cu_xO_yH_z}^{Cu}$ atmosphere and in an N2O atmosphere are given in Supporting Information, Section S3. Phase diagrams for O2 and N2O, including all four dimer anchoring configurations and monomer anchoring configurations 1Al and 2Al-A are shown in Figure 2 (a)-(d). A complete set of all possible phase diagrams for an O₂ atmosphere containing only a single dimer anchoring configuration can be found in our past study,²⁵ while a full set of phase diagrams for N₂O containing only a single dimer anchoring configuration is shown in Supporting Information, Figure S5. Additionally, $\mu^{Cu}_{Cu_xO_yH_z}$ for all Cu species at activation and reaction conditions in an O₂ and N₂O atmosphere are shown in Figures S6 and S7 in the Supporting Information. Comparing these two sets of conditions, we find that under reaction conditions in the stepwise conversion process for methane to methanol, the hydroxylated Cu dimers Cu₂O₂H₂ and Cu₂OH are stabilized in an O₂ atmosphere, while Cu₂O₂ sites are stabilized in an N₂O atmosphere (see Figure 2 (f)). An analysis of the orbital diagrams of selected sites (see Supporting Information section S6) indicates that in an N₂O atmosphere, Cu dimers with higher oxidation states of Cu are stabilized compared to O₂. This agrees with the intuitive understanding that the presence of a stronger oxidant (N₂O compared to O_2) leads to the formation of sites with a higher oxidation state of Cu. We furthermore see that for the 2Al-A configuration for monomer anchoring, where two Al atoms are located at opposite ends of the same six-ring of the zeolite structure, Cu monomers are preferred for both types of activation for many monomer and dimer anchoring configuration combinations, which is undesirable for the conversion of methane to methanol (see Figure 2 (b) and Figure S5 in the Supporting Information). Lastly, we emphasize that in an experimental setup, changing gas pressures is a fast process, while heating or cooling is comparatively slow. Phase diagrams for dimer anchoring configuration D-A in an O₂ environment imply that the preferred Cu site changes from A-Cu₂OH present at activation conditions to A-Cu₂O₂H₂ at reaction conditions (see Figure 2 (e)). Cooling in the presence of the oxidant will increase the time the system is exposed to conditions where the thermodynamically preferred site at reaction conditions is most stable. This protocol helps to mitigate potential kinetic restrictions for site formation and helps to ensure that the thermodynamically favored site is indeed present under reaction conditions.

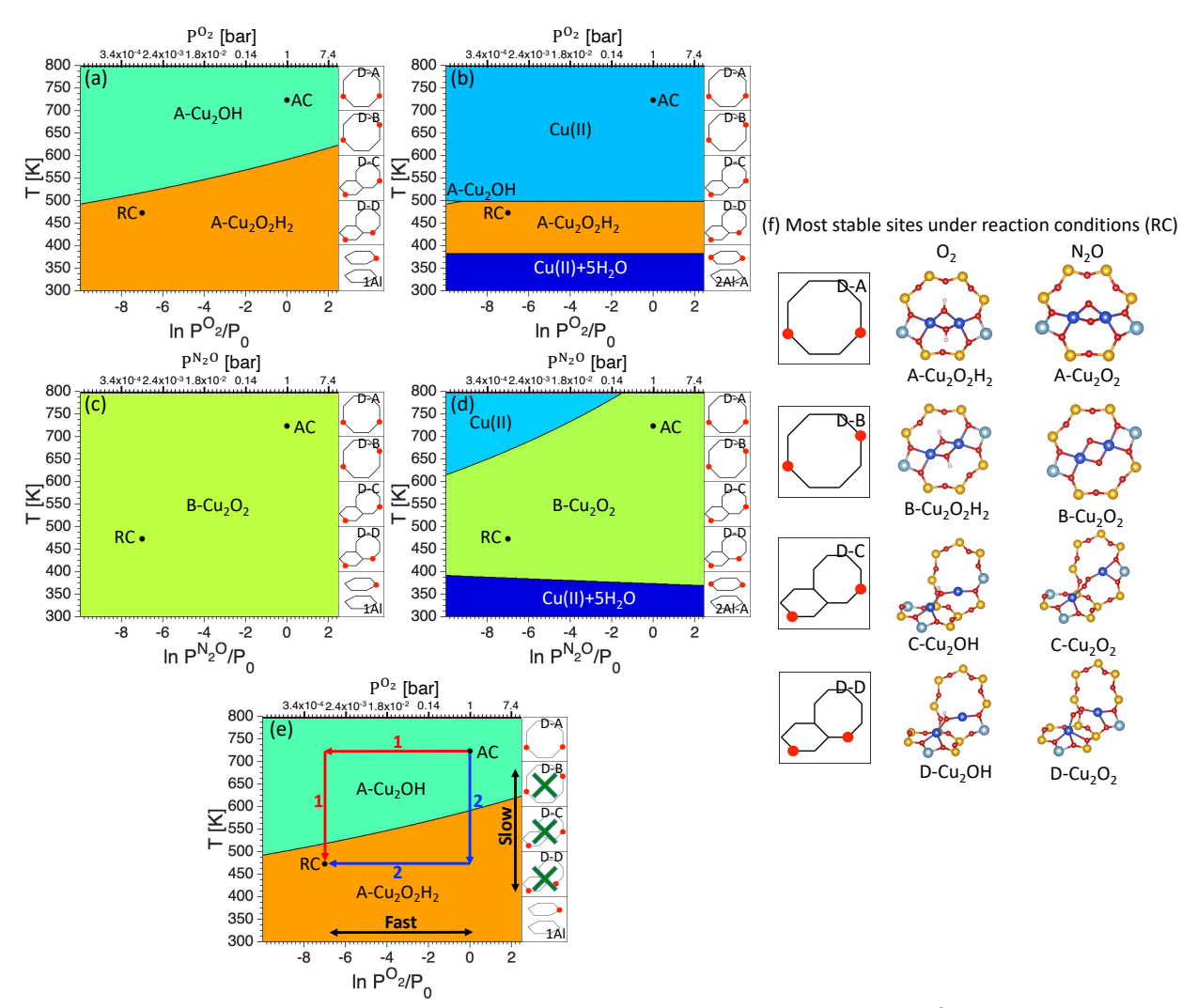


Figure 2: (a)-(d): Phase diagrams for Cu-exchanged SSZ-13 with respect to P^{O_2} and T ((a), (b), and (e)), and P^{N_2O} and T ((c) and (d)) for all four dimer exchange sites and monomer exchange sites 1AI ((a), (c)) and 2AI-A ((b), (d)). The standard pressure P_0 is defined as 1 bar. The thermodynamically preferred sites are indicated by regions of identical color, and the site type is indicated by the labels. The included AI configurations are indicated by schematic representations on the right side of the phase diagrams, which correspond to Figure 1. In (a) through (d), activation conditions (AC) and reaction conditions (RC) are marked by a black dot. (e): Potential reaction paths in the stepwise conversion with respect to P^{O_2} and T. In path 1, marked by red arrows and labeled 1, first P^{O_2} is reduced, and then the system is cooled, while in path 2, marked by blue arrows and labeled, the system is first cooled in O_2 and then P^{O_2} is reduced. (f): The most stable sites for activation in O_2 and O_2 for the four different dimer exchange sites under reaction conditions (RC). In atomistic representations, O_2 is shown in yellow, O_2 in red, O_3 in grey, O_3 in blue, and O_3 in white, respectively. Schematic representations of dimer/trimer exchange sites correspond to Figure 1. (For detailed explanations of phase diagram legends, see Figure S14 in the SI.

Based on the points discussed above, we can derive three design principles for Cu-SSZ-13 in the stepwise conversion of methane to methanol from phase diagrams: (i) changing the oxidizing agent during catalyst activation from O_2 to N_2O will change Cu sites from hydroxylated to Cu-oxo dimers, (ii) the pairing of Al atoms in the same six-ring should be avoided to maximize Cu dimer formation, and (iii) when cooling the material after catalyst activation, it should still be exposed to the oxidizing agent to mitigate potential kinetic barriers for site formation and ensure that thermodynamically preferred sites are present when the reaction starts.

Characterization: To confirm these theoretical predictions, we relied on experimental measurements. Following a synthesis protocol that minimizes Al pairing, we synthesized SSZ-13 with a Si/Al ratio of 14.7^{26,50}. After ion exchange with Cu(CO₂CH₃)₂, we arrived at a sample with a Cu/Al ratio of 0.41. The experimental protocol is given in Supporting Information, Sections S1.1.1 and S1.1.2. Subsequently, we activated the zeolite to 723 K in either O₂ or N₂O and cooled the sample in the oxidizing agent to room temperature. We characterized the zeolite using UV-vis-NIR spectroscopy and compared experimental spectra to our previous theoretical predictions obtained by using a combination of time-dependent density functional theory in combination with spin orbit coupling²⁶. Following activation in O₂, the sample showed a broad signal below 20500 cm⁻¹ with three distinct shoulders at 11500 cm⁻¹, 13400 cm⁻¹, 16230 cm⁻¹, as well as weak shoulders at 20000 cm⁻¹, and 21600 cm⁻¹ (see Figure 3 (a)). These signals can be explained by a combination of theoretically predicted signals from three different hydroxylated Cu-dimer sites predicted to be most stable in phase diagrams for the different hydroxylated Cu-dimer exchange sites²⁶, namely A-Cu₂O₂H₂, B-Cu₂O₂H₂, and D-Cu₂OH, as well as signals of a Cu monomers bound to a silanol defect, but not by signals of various Cu-oxo dimers. Additionally, the high wavenumber peak around 41000 cm⁻¹ is assigned to Cu monomers.

Following activation in N_2O and cooling the system to room temperature in the presence of the oxidizing agent, a different picture emerged (see Figure 3 (a)). While there is also a signal in the low wavenumber range with shoulders at $11500~\rm cm^{-1}$ and $13400~\rm cm^{-1}$, the main difference resulting from activation in N_2O is a broadening of the high wavenumber peak in the 29000 cm⁻¹ to $37000~\rm cm^{-1}$ range. To better illustrate these differences, we show the difference in UV-vis NIR spectra after activation in O_2 and N_2O in the Supporting Information, Figure S8. Comparing these results to theoretically predicted optical spectra for Cu-oxo dimers reported in the literature (see Figure 3 (a)), we find that this broadening corresponds to the signal of the $A-Cu_2O_2$ and $B-Cu_2O_2$ sites. Further, the $A-Cu_2O_2$ site is responsible for the signal at $13400~\rm cm^{-1}$, and again we attribute the remaining signal at $11500~\rm cm^{-1}$ to a defect bound Cu monomer. Notably, we do not find any signals associated with $C-Cu_2O_2$ or $D-Cu_2O_2$, the predicted most stable sites for dimer exchange positions bridging the six-ring and eight-ring. However, an additional signal of Cu monomers is observed in the UV-vis-NIR difference spectrum (Figure S8 in the Supporting Information). This indicates that $C-Cu_2O_2$ and $D-Cu_2O_2$ sites might not be present after activation in N_2O .

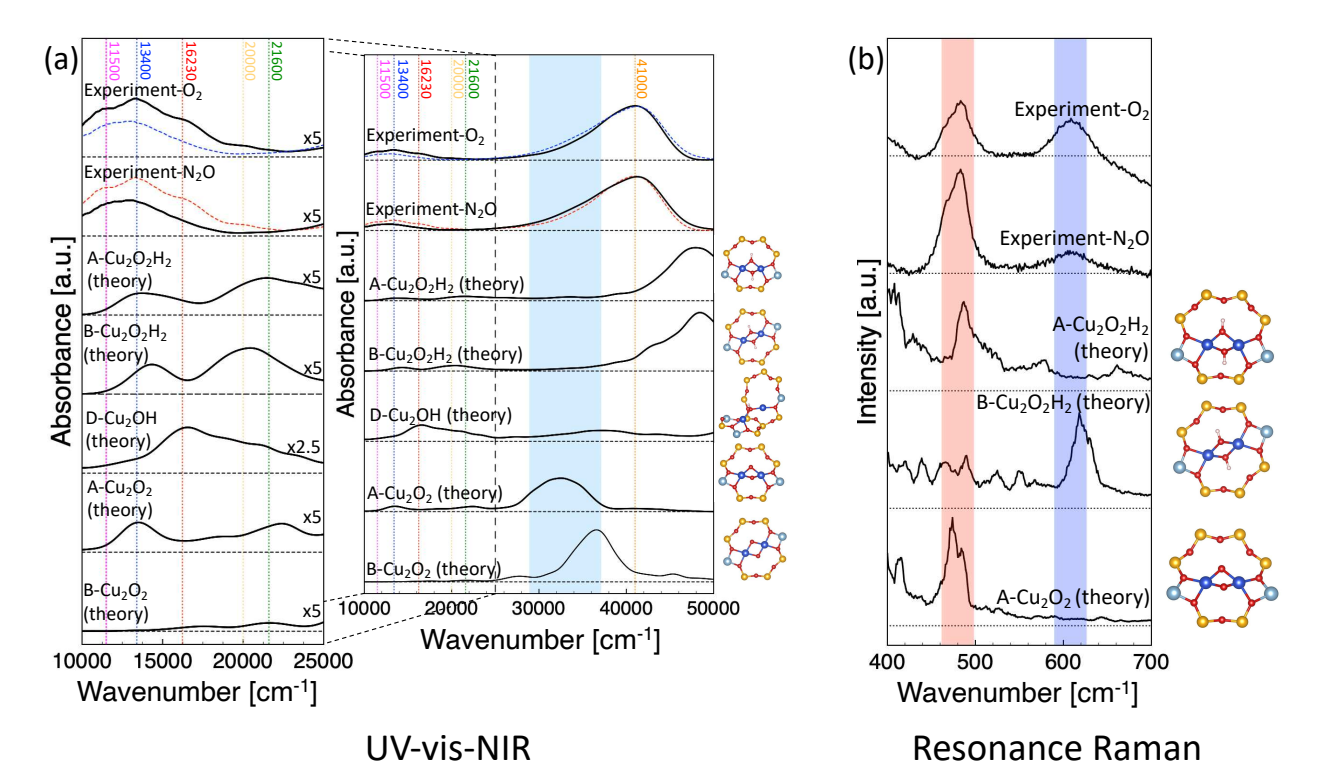


Figure 3: (a): Experimentally measured UV-vis-NIR spectra after activation and cooling to room temperature in O_2 (Experiment- O_2) and N_2O (Experiment- N_2O), and theoretically predicted optical spectra for the Cu dimers A-Cu₂O₂H₂, B-Cu₂O₂H₂, D-Cu₂OH, A-Cu₂O₂, and B-Cu₂O₂ (atomic structures shown to the right of the respective spectra). Experimentally, spectra were measured in a glove box atmosphere. For better readability, the full spectrum is shown on the right, and magnified spectra in the 10,000 cm⁻¹ to 25,000 cm⁻¹ range are shown on the left. Spectra are displayed as black, solid lines, and peak positions are marked by dashed, vertical lines. Numerical values are given in the vertical color legend. Additionally, the blue shaded area marks a region where a peak broadening is seen in experiments. For comparison, experimental spectra for activation in N_2O and O_2 are given as blue and red dashed lines (near the top of the left panel), respectively. (b): Experimentally measured Resonance Raman spectra after activation in O2 (Experiment-O₂) and N₂O (Experiment-N₂O) after cooling to reaction conditions (T=473 K) in oxidizing agent flow, as well as theoretically modeled Raman spectra for selected Cu dimers (A- $Cu_2O_2H_2$, B- $Cu_2O_2H_2$, and A- Cu_2O_2 ; atomic structures shown to the right of the respective spectra). Spectra are shown as black, solid lines and peak positions are marked by blue and red shaded areas, respectively. The color code of atomistic representations in A and B corresponds to Figure 2.

To further characterize our Cu-SSZ-13 sample, we turned to Raman spectroscopy. Again, we initially activated the system in O₂ or N₂O at 723 K, cooled the system to reaction conditions (T=473 K) in oxidizing agent flow, and collected the Raman spectra (see Figure 3 (b)). Using a Raman laser with a wavelength of 785 nm ensured that we optically excite vibrations associated with Cu-oxo or Cu-hydroxy dimers. For both oxidizing agents we identified well-defined signals around 485 cm⁻¹ and 615 cm⁻¹. After activation in O₂, the intensities of both signals were comparable. However, the 485 cm⁻¹ signal was by a factor of 6.5 stronger in intensity compared

to the signal at 615 cm⁻¹ after activation in N₂O than that in O₂. To understand these signals, we modeled Raman spectra of the most stable Cu-oxo and Cu-hydroxy dimers by Fourier transformation of the velocity autocorrelation function of the Cu-O distances in the dimers obtained from molecular dynamics simulations⁵¹. Relevant spectra are shown in Figure 3 (b), and Raman spectra of the other dimer structures as well as computational details are given in Supporting Information, Section 1.2.2 and Figure S9, respectively. In all assignments, we focus on major peaks to avoid overinterpretation of spectra. Our simulations show that A-Cu₂O, A-Cu₂O₂ and A-Cu₂O₂H₂ are characterized by significant, broad signals with maxima between 467 cm⁻¹ and 487 cm⁻¹, respectively, while B-Cu₂O₂H₂ has a characteristic signal at 615 cm⁻¹. In combination with information from phase diagrams and UV-vis-NIR spectroscopy, we assign the experimental spectrum observed after activation in O₂ to A-Cu₂O₂H₂ and B-Cu₂O₂H₂, the most stable Cu sites at reaction conditions for dimer anchoring configurations D-A and D-B in the eight-ring (Figure 2, (a) and (b) and phase diagrams published in the literature²⁵). For activation in N₂O, we assign the experimental signal around 485 cm⁻¹ to A-Cu₂O₂, the most stable Cu dimer sites for dimer exchange site D-A at N₂O reaction conditions (Figure 2, (c) and (d), and Figure S5 in Supporting Information). The origin of the weak signal at 615 cm⁻¹ could again be assigned to B-Cu₂O₂H₂, which, depending on the exact conditions, could be formed as a minority species. Notably, we cannot exclude the presence of a spectator Cu species or a weak framework vibration leading to the signal at 615 cm⁻¹. Importantly, the three Cu dimers used in our peak assignments are optically active at 785 nm (12740 cm⁻¹), while other sites that we do not observe in our measurements are inactive for optical activation at this specific wavelength.

Reactivity: So far, a combination of phase diagrams, UV-vis-NIR, and Raman spectroscopy point towards a change in the stoichiometry and geometry of Cu dimers with the applied oxidizing agent, namely the presence of hydroxylated Cu dimers after activation in O2 and the presence of Cu-oxo dimers after activation in N₂O. To understand the impact of Cu-site stoichiometry on methane conversion, we subsequently evaluated the ability of the zeolite to convert methane to methanol in a stepwise process using these two distinct activation protocols. Similar to the treatment protocol used above, we (i) activated the zeolite at 723 K in O₂ or N₂O for 8 hours, (ii) cooled to 473 K in the presence of the respective oxidizing agent, (iii) exposed the system to methane for 2 hours at 473 K, (iii) purged excessive CH₄ using He, and (iv) extract methanol via H₂O vapor. A detailed experimental protocol is given in Supporting Information, Section S1.1.5. Following this protocol, we found that activation in both oxidizing agents leads to similar, small amounts of CO, CO₂, and di-methyl ether (DME) (3.03 μmol/g CO, 1.47 μmol/g CO₂, 0.25 μmol/g DME after activation in O₂ and 3.09 µmol/g CO, 2.66 µmol/g CO₂, 0.27 µmol/g DME after activation in N2O, respectively; see Figure 4 (a)). We attribute the presence of products besides methanol to either catalytic methanol oxidation⁵³ or methanol coupling to DME over Bronsted acid sites⁵⁴ during the extraction process. However, the zeolite produces more than twice as much methanol after activation in N₂O (23.23 μmol/g) compared to activation in O₂ (9.55 μmol/g). Even if taking the methane conversion into all observed products into account, activation in O₂ leads to a total conversion of 14.55 μmol/g of methane, while activation in N₂O leads to a total conversion of 29.52 μmol/g. At the same time, conversion numbers indicate that only a small amount of Cu is active in the conversion of methane. This indicates that our zeolite only contains a limited number of exchange positions where sites can form that are active in the conversion of methane to methanol.

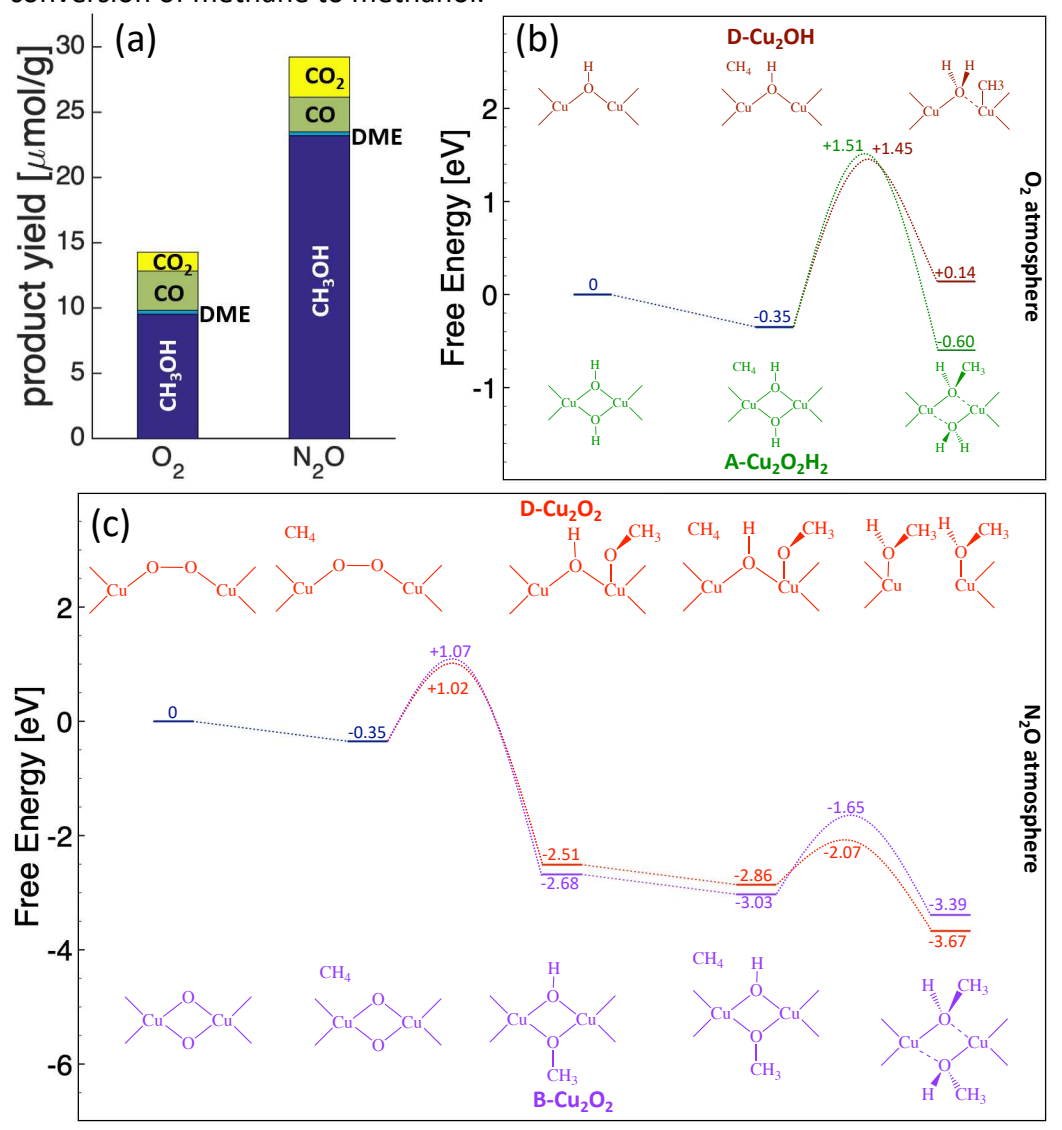


Figure 4: (a): Experimentally measured conversion of methane per cycle after activation in O_2 and in N_2O . (b) and (c): Calculated Free Energy diagrams at 473 K for the conversion of methane to methanol for four distinct active sites: $A-Cu_2O_2H_2$ ((b), green), $D-Cu_2OH$ ((b), dark red), $B-Cu_2O_2$ ((c), purple), and $D-Cu_2O_2$ ((c), red). Maximum in curved lines denotes a transition state. For each reaction, reaction intermediates are schematically displayed, and energies are reported as Gibbs' Free Energies in eV. Atomistic representations of intermediates of partial reactions, transition states, and of intermediates, and preferred spin states are provided in Supporting Information, section S5.

This difference in methane conversion suggests that the active site structure significantly influences the ability of Cu dimers to convert methane to methanol. To rationalize this difference in catalytic performance, we studied the energetics of the reaction pathways for the conversion of methane to methanol over four different site structures that are stabilized under the specified

experimental protocols. More specifically, we focused on A-Cu₂O₂H₂ and D-Cu₂OH, the most stable sites for activation in O₂ (see Figure S6 in the Supporting Information), for sites located in the eight-membered ring or bridging six- and eight-membered rings, respectively. We also studied B-Cu₂O₂ and D-Cu₂O₂, two sites that are most stable after activation in N₂O for the two different site geometries in SSZ-13. Since the system is kept at fixed conditions for an extended period during activation, we assume that the system is thermodynamically equilibrated. In the analysis of the free energy diagrams, we therefore first focus on the reaction energy as a measure of whether methane will be converted to methanol. Subsequently, we calculated the activation energy to understand the reaction kinetics. For all pathways, different spin states were evaluated for all intermediates and transition states; only the lowest energy spin states are reported. For some of the sites, conversion of methane to methanol is a multi-step process. Only the energies of the initial and final states and the effective activation energy are shown in the main text. All partial reactions studied, atomistic representations of intermediates, and preferred spin states are provided in Supporting Information, Section S7. Atomistic structure files for all relevant intermediates and transition states are provided in the supporting structures file. Details of the computational strategy are given in Supporting Information, Section S1.2.3.

Conversion of methane over the two Cu-dimers stabilized in an O_2 atmosphere varies significantly (see Figure 4 (b) and Figures S10 and S11 in Supporting Information). Only methane conversion over A-Cu₂O₂H₂, where methane is converted to methanol and a water molecule, shows a negative reaction energy (-0.60 eV). For D-Cu₂OH, on the other hand, where methane is converted to a methyl group bound to a Cu atom of the dimer and a water molecule, the reaction energy is positive (+0.14 eV). Even though both sites show similar activation energies of 1.86 eV and 1.80 eV, respectively, the reaction energies imply that only the Cu-dihydroxyl dimer can convert one methane molecule to methanol.

The situation for the two Cu-dimers stabilized in an N_2O atmosphere is different (see Figure 4 (c) and Figures S12 and S13 in Supporting information). Here, the conversion of the first methane molecule is favored and, in both cases, a Cu-dimer with one hydroxyl- and one methoxy-group is formed. Reaction energies are vastly negative (-2.33 eV and -2.16 eV, respectively), and activation energies are reasonably low (1.37 eV and 1.42 eV, respectively). The resulting sites have the potential to convert a second methane molecule. Again, both sites show a negative reaction energy (-0.81 eV and -0.36, respectively) and a low activation energy for methane conversion (0.79 eV and 1.38 eV, respectively) and will therefore convert a second methane molecule.

At the same time, the analysis of the reaction energy for the conversion of methane over the Cu-OH monomer is positive (+0.38 eV), which indicates that this site, which represents the majority of Cu species in our zeolite sample, as indicated by UV-vis spectra in Figure 3 (a), is inactive for the conversion of methane to methanol.

Discussion and Conclusions:

We can now use these insights to rationalize the experimentally observed differences in methane conversion between O_2 and N_2O as oxidizing agents: In O_2 , hydroxylated Cu dimers are stabilized,

which, depending on their location in the zeolite framework and their exact stoichiometry, can convert either one or zero methane molecules to methanol. In N_2O , however, Cu-dioxo-dimers are stabilized, which, depending on their exact structure, can convert two methane molecules. Therefore, when N_2O is used as the oxidizing agent, more than twice as much methane will be converted to methanol compared to when O_2 is used as the oxidizing agent. Interestingly, A- $Cu_2O_2H_2$ shows turnover rates of about one methane molecule per hour, a conversion rate that agrees well with experimental measurements in the literature⁴⁰.

In the past, the impact of active site structure of Cu site structure on the conversion of methane to methanol has been widely discussed^{9,13,14,16,17,20,21,29,30,34,35,52,55–59}. However, in most cases the focus was only on Cu-oxo sites and the conversion of the first methane molecule. The present study goes beyond this limit and asks how many methane molecules each active site can convert. The reaction paths analyzed in this work indicate that bond formation between H or CH₃ and Cu is endothermic compared to CH₄ and a sufficient number of O or OH groups need to be available to accommodate these reaction intermediates. This implies that there may be a more general structure/property relationship for the conversion of methane to methanol over small Cu-oxo and hydroxy clusters. More specifically, at least two hydroxyl groups are necessary to allow for the formation of one methanol and one water molecule, while only one oxo group is required to achieve a similar conversion. These findings indicate that at least two hydroxy groups or one oxo group must be present in a small transition metal cluster to convert one methane molecule to methanol. We suggest that this simple rule provides an intuitive understanding of the ability of small transition metal-oxo and transition metal-hydroxy clusters in zeolites to convert methane to methanol. Further experimentation with other metals, zeolites, and reaction conditions³⁷ will be needed to develop additional insights for the design of zeolite catalysts for the efficient conversion of methane to methanol.

Acknowledgements: This work was supported by the National Science Foundation, grant number CHE-1800284. The authors thank Dr. Lang Xu and Dr. Mark Figueras Valls (both UW Madison) for comments on the manuscript. We acknowledge computational time at the National Energy Research Scientific Computing Center (NERSC), a DOE Office of Science User Facility supported by the Office of Science of the U.S. Department of Energy, contract DE-AC02-05CH11231 using NERSC awards BES-ERCAP0022773 and BES-ERCAP0024425. Part of the computational work was carried out using supercomputing resources at the Center for Nanoscale Materials (CNM), a DOE Office of Science User Facility located at Argonne National Laboratory that is supported by DOE contract DE-AC02-06CH11357.

List of Supporting Information: Supporting Information contains methods, trimer structures and spins, phase diagrams, site stability comparison, UV-vis NIR difference spectra, , theoretically predicted Raman spectra, reaction pathway analysis for methane conversion, and a legend for phase diagrams.

References:

- (1) Jahangiri, H.; Bennett, J.; Mahjoubi, P.; Wilson, K.; Gu, S. A Review of Advanced Catalyst Development for Fischer-Tropsch Synthesis of Hydrocarbons from Biomass Derived Syn-Gas. *Catal. Sci. Technol.* **2014**, *4* (8), 2210–2229.
- (2) Luk, H. T.; Mondelli, C.; Ferré, D. C.; Stewart, J. A.; Pérez-Ramírez, J. Status and Prospects in Higher Alcohols Synthesis from Syngas. *Chem. Soc. Rev.* **2017**, *46* (5), 1358–1426.
- (3) Grabow, L. C.; Mavrikakis, M. Mechanism of Methanol Synthesis on Cu through CO₂ and CO Hydrogenation. *ACS Catal.* **2011**, *1*, 365–384.
- (4) Latimer, A. A.; Kakekhani, A.; Kulkarni, A. R.; Nørskov, J. K. Direct Methane to Methanol: The Selectivity-Conversion Limit and Design Strategies. *ACS Catal.* **2018**, *8* (8), 6894–6907.
- (5) Ravi, M.; Sushkevich, V. L.; Knorpp, A. J.; Newton, M. A.; Palagin, D.; Pinar, A. B.; Ranocchiari, M.; Bokhoven, J. A. Van. Misconceptions and Chellenges in Methane-to-Methanol over Transition-Metal-Exchanged Zeolites. *Nat. Catal.* **2019**, *2*, 485–494.
- (6) Dinh, K. T.; Sullivan, M. M.; Serna, P.; Meyer, R. J.; Dincă, M.; Román-Leshkov, Y. Viewpoint on the Partial Oxidation of Methane to Methanol Using Cu- and Fe-Exchanged Zeolites. *ACS Catal.* **2018**, *8* (9), 8306–8313.
- (7) Vanelderen, P.; Vancauwenbergh, J.; Sels, B. F.; Schoonheydt, R. A. Coordination Chemistry and Reactivity of Copper in Zeolites. *Coord. Chem. Rev.* **2013**, *257* (2), 483–494.
- (8) Snyder, B. E. R.; Bols, M. L.; Schoonheydt, R. A.; Sels, B. F.; Solomon, E. I. Iron and Copper Active Sites in Zeolites and Their Correlation to Metalloenzymes. *Chmical Rev.* **2018**, *118*, 2718–2768.
- (9) Latimer, A. A.; Kulkarni, A. R.; Aljama, H.; Montoya, J. H.; Yoo, J. S.; Tsai, C.; Abild-Pedersen, F.; Studt, F.; Nørskov, J. K. Understanding Trends in C-H Bond Activation in Heterogeneous Catalysis. *Nat. Mater.* **2017**, *16* (2), 225–229.
- (10) Snyder, B. E. R.; Vanelderen, P.; Bols, M. L.; Hallaert, S. D.; Böttger, L. H.; Ungur, L.; Pierloot, K.; Schoonheydt, R. A.; Sels, B. F.; Solomon, E. I. The Active Site of Low-Temperature Methane Hydroxylation in Iron-Containing Zeolites. *Nat. Publ. Gr.* **2016**, *536* (7616), 317–321.
- (11) Snyder, B. E. R.; Bols, M. L.; Rhoda, H. M.; Plessers, D.; Schoonheydt, R. A.; Sels, B. F.; Solomon, E. I. Cage Effects Control the Mechanism of Methane Hydroxylation in Zeolites. *Science (80-.).* **2021**, *373* (6552), 327–331.
- (12) Bols, M. L.; Snyder, B. E. R.; Rhoda, H. M.; Cnudde, P.; Fayad, G.; Schoonheydt, R. A.; Van Speybroeck, V.; Solomon, E. I.; Sels, B. F. Coordination and Activation of Nitrous Oxide by Iron Zeolites. *Nat. Catal.* **2021**, *4* (4), 332–340.
- (13) Rhoda, H. M.; Plessers, D.; Heyer, A. J.; Bols, M. L.; Schoonheydt, R. A.; Sels, B. F.; Solomon, E. I. Spectroscopic Definition of a Highly Reactive Site in Cu-CHA for Selective Methane Oxidation: Tuning a Mono-μ-Oxo Dicopper (II) Active Site for Reactivity. *J. Am. Chem. Soc.* **2021**, *143*, 7531–7540.
- (14) Woertink, J. S.; Smeets, P. J.; Groothaert, M. H.; Vance, M. A.; Sels, B. F.; Schoonheydt, R. A.; Solomon, E. I. A [Cu₂O]²⁺ Core in Cu-ZSM-5, the Active Site in the Oxidation of Methane to Methanol. *Proc. Natl. Acad. Sci.* 2009, 106, 18908–18913.

- (15) Ipek, B.; Wulfers, M. J.; Kim, H.; Göltl, F.; Hermans, I.; Smith, J. P.; Booksh, K. S.; Brown, C. M.; Lobo, R. F. Formation of [Cu₂O₂]²⁺ and [Cu₂O]²⁺ toward C-H Bond Activation in Cu-SSZ-13 and Cu-SSZ-39. ACS Catal. 2017, 7 (7), 4291–4303.
- (16) Sushkevich, V. L.; Palagin, D.; Ranocchiari, M.; Bokhoven, J. A. Van. Selective Anaerobic Oxidation of Methane Enables Direct Synthesis of Methanol. *Science* (80-.). 2017, 356, 523–527.
- (17) Grundner, S.; Markovits, M. A. C.; Li, G.; Tromp, M.; Pidko, E. A.; Hensen, E. J. M.; Jentys, A.; Sanchez-Sanchez, M.; Lercher, J. A. Single-Site Trinuclear Copper Oxygen Clusters in Mordenite for Selective Conversion of Methane to Methanol. *Nat. Commun.* **2015**, *6*, 7546.
- (18) Bregante, D. T.; Wilcox, L. N.; Liu, C.; Paolucci, C.; Gounder, R.; Flaherty, D. W. Dioxygen Activation Kinetics over Distinct Cu Site Types in Cu-Chabazite Zeolites. *ACS Catal.* **2021**, *11*, 11873–11884.
- (19) Brezicki, G.; Kammert, J. D.; Gunnoe, T. B.; Paolucci, C.; Davis, R. J. Insights into the Speciation of Cu in the Cu-H-Mordenite Catalyst for the Oxidation of Methane to Methanol. *ACS Catal.* **2019**, *9*, 5308–5319.
- (20) Brezicki, G.; Zheng, J.; Paolucci, C.; Schlögl, R.; Davis, R. J. Effect of the Co-Cation on Cu Speciation in Cu-Exchanged Mordenite and ZSM-5 Catalysts for the Oxidation of Methane to Methanol. *ACS Catal.* **2021**, *11* (9), 4973–4987.
- (21) Pappas, D. K.; Borfecchia, E.; Dyballa, M.; Pankin, I.; Lomachenko, K. A.; Martini, A.; Signorile, M.; Teketel, S.; Arstad, B.; Berlier, G.; et al. Methane to Methanol: Structure-Activity Relationships for Cu-CHA. *J. Am. Chem. Soc.* **2017**, *139*, 14961–14975.
- (22) Pappas, D. K.; Martini, A.; Dyballa, M.; Kvande, K.; Teketel, S.; Lomachenko, K. A.; Baran, R.; Glatzel, P.; Arstad, B.; Berlier, G.; et al. The Nuclearity of the Active Site for Methane to Methanol Conversion in Cu-Mordenite: A Quantitative Assessment. *J. Am. Chem. Soc.* **2018**, *140*, 15270–15278.
- (23) Li, H.; Paolucci, C.; Khurana, I.; Wilcox, L. N.; Göltl, F.; Albarracin-Caballero, J. D.; Shih, A. J.; Ribeiro, F. H.; Gounder, R.; Schneider, W. F. Consequences of Exchange-Site Heterogeneity and Dynamics on the UV-Visible Spectrum of Cu-Echanged SSZ-13. *Chem. Sci.* **2019**, *10*, 2373–2384.
- (24) Wijerathne, A.; Sawyer, A.; Daya, R.; Paolucci, C. Competition between Mononuclear and Binuclear Copper Sites across Different Zeolite Topologies. *JACS Au* **2024**, *4*, 197–215.
- (25) Göltl, F.; Bhandari, S.; Mavrikakis, M. Thermodynamics Perspective on the Stepwise Conversion of Methane to Methanol over Cu-Exchanged SSZ-13. ACS Catal. 2021, 11, 7719–7734.
- (26) Göltl, F.; Bhandari, S.; Lebron-Rodriguez, E.; Gold, J.; Zones, S. I.; Hermans, I.; Dumesic, J.; Mavrikakis, M. Identifying Hydroxylated Copper Dimers in SSZ-13 via UV-Vis-NIR Spectroscopy. *Catal. Sci. Technol.* 2022, DOI: 10.1039/d2cy00353h.
- (27) Narsimhan, K.; Iyoki, K.; Dinh, K.; Román-Leshkov, Y. Catalytic Oxidation of Methane into Methanol over Copper-Exchanged Zeolites with Oxygen at Low Temperature. *ACS Cent. Sci.* **2016**, *2* (6), 424–429.
- (28) Xiao, P.; Wang, Y.; Lu, Y.; De Baerdemaeker, T.; Parvulescu, A. N.; Müller, U.; De Vos, D.; Meng, X.; Xiao, F. S.; Zhang, W.; et al. Effects of Al Distribution in the Cu-Exchanged AEI Zeolites on the Reaction Performance of Continuous Direct Conversion of Methane to

- Methanol. Appl. Catal. B Environ. 2023, 325 (December 2022).
- (29) Groothaert, M. H.; Smeets, P. J.; Sels, B. F.; Jacobs, P. A.; Schoonheydt, R. A. Selective Oxidation of Methane by the Bis(μ-Oxo)Dicopper Core Stabilized on ZSM-5 and Mordenite Zeolites. J. Am. Chem. Soc. 2005, 127 (5), 1394–1395.
- (30) Vanelderen, P.; Snyder, B. E. R.; Tsai, M.-L.; Hadt, R. G.; Vancauwenbergh, J.; Coussens, O.; Schoonheydt, R. A.; Sels, B. F.; Solomon, E. I. Spectroscopic Definition of the Copper Active Sites in Mordenite: Selective Methane Oxidation. *J. Am. Chem. Soc.* **2015**, *137* (19), 6383–6392.
- (31) Prodinger, S.; Kvande, K.; Arstad, B.; Borfecchia, E.; Beato, P.; Svelle, S. Synthesis—Structure—Activity Relationship in Cu-MOR for Partial Methane Oxidation: Al Siting via Inorganic Structure-Directing Agents. *ACS Catal.* **2022**, 2166–2177.
- (32) Engedahl, U.; Grönbeck, H.; Hellman, A. First-Principles Study of Oxidation State and Coordination of Cu-Dimers in Cu-SSZ-13 during Methane-to-Methanol Reaction Conditions. *J. Phys. Chem. C* **2019**, *123* (43), 26145–26150.
- (33) Kulkarni, A. R.; Zhao, Z. J.; Siahrostami, S.; Nørskov, J. K.; Studt, F. Monocopper Active Site for Partial Methane Oxidation in Cu-Exchanged 8MR Zeolites. *ACS Catal.* **2016**, *6* (10), 6531–6536.
- (34) Knorpp, A. J.; Pinar, A. B.; Baerlocher, C.; McCusker, L. B.; Casati, N.; Newton, M. A.; Checchia, S.; Meyet, J.; Palagin, D.; van Bokhoven, J. A. Paired Copper Monomers in Zeolite Omega: The Active Site for Methane-to-Methanol Conversion. *Angew. Chemie Int. Ed.* **2021**, *60* (11), 5854–5858.
- (35) Heyer, A. J.; Plessers, D.; Braun, A.; Rhoda, H. M.; Bols, M. L.; Hedman, B.; Hodgson, K. O.; Schoonheydt, R. A.; Sels, B. F.; Solomon, E. I. Methane Activation by a Mononuclear Copper Active Site in the Zeolite Mordenite: Effect of Metal Nuclearity on Reactivity. *J. Am. Chem. Soc.* **2022**, *144* (42), 19305–19316.
- (36) Lee, I.; Lee, M.-S.; Tao, L.; Ikuno, T.; Khare, R.; Jentys, A.; Huthwelker, T.; Borca, C. N.; Kalinko, A.; Gutiérrez, O. Y.; et al. Activity of Cu–Al–Oxo Extra-Framework Clusters for Selective Methane Oxidation on Cu-Exchanged Zeolites. *JACS Au* **2021**, *1* (9), 1412–1421.
- (37) Tao, L.; Khramenkova, E.; Lee, I.; Ikuno, T.; Khare, R.; Jentys, A.; Fulton, J. L.; Kolganov, A. A.; Pidko, E. A.; Sanchez-Sanchez, M.; et al. Speciation and Reactivity Control of Cu-Oxo Clusters via Extraframework Al in Mordenite for Methane Oxidation. *J. Am. Chem. Soc.* **2023**, *145* (32), 17710–17719.
- (38) Göltl, F. Three Grand Challenges for the Computational Design of Heterogeneous Catalysts. *J. Phys. Chem. C* **2022**, *126* (7), 3305–3313.
- (39) Göltl, F.; Conrad, S.; Wolf, P.; Müller, P.; Love, A. M.; Burt, S. P.; Wheeler, J. N.; Hamers, R. J.; Hummer, K.; Kresse, G.; et al. UV–Vis and Photoluminescence Spectroscopy to Understand the Coordination of Cu Cations in the Zeolite SSZ-13. *Chem. Mater.* **2019**, *31*, 9582–9592.
- (40) Pappas, D. K.; Borfecchia, E.; Dyballa, M.; Pankin, I. A.; Lomachenko, K. A.; Martini, A.; Signorile, M.; Teketel, S.; Arstad, B.; Berlier, G.; et al. Methane to Methanol: Structure-Activity Relationships for Cu-CHA. *J. Am. Chem. Soc.* **2017**, *139* (42), 14961–14975.
- (41) Paolucci, C.; Khurana, I.; Parekh, A. A.; Li, S.; Shih, A. J.; Li, H.; Iorio, J. R. Di; Albarracin-caballero, J. D.; Yezerets, A.; Miller, J. T.; et al. Dynamic Multinuclear Sites Formed by Mobilized Copper Ions in NO_x Selective Catalytic Reduction. *Science (80-.).* **2017**, *5630*,

- 1-11.
- (42) Borfecchia, E.; Beato, P.; Svelle, S.; Olsbye, U.; Lamberti, C.; Bordiga, S. Cu-CHA-a Model System for Applied Selective Redox Catalysis. *Chem. Soc. Rev.* **2018**, *47* (22), 8097–8133.
- (43) Krishna, S. H.; Goswami, A.; Wang, Y.; Jones, C. B.; Dean, D. P.; Miller, J. T.; Schneider, W. F.; Gounder, R. Influence of Framework Al Density in Chabazite Zeolites on Copper Ion Mobility and Reactivity during NOx Selective Catalytic Reduction with NH3. *Nat. Catal.* 2023, 6 (3), 276–285.
- (44) Xie, P.; Pu, T.; Aranovich, G.; Guo, J.; Donohue, M.; Kulkarni, A.; Wang, C. Bridging Adsorption Analytics and Catalytic Kinetics for Metal-Exchanged Zeolites. *Nat. Catal.* **2021**, *4*, 144–156.
- (45) Becher, J.; Sanchez, D. F.; Doronkin, D. E.; Zengel, D.; Meira, D. M.; Pascarelli, S.; Grunwaldt, J.-D.; Sheppard, T. L. Chemical Gradients in Automotive Cu-SSZ-13 Catalysts for NOx Removal Revealed by Operando X-Ray Spectrotomography. *Nat. Catal.* **2021**, *4* (1), 46–53.
- (46) Göltl, F.; Sautet, P.; Hermans, I. The Impact of Finite Temperature on the Coordination of Cu Cations in the Zeolite SSZ-13. *Catal. Today* **2016**, *267*, 41–46.
- (47) Paolucci, C.; Parekh, A. A.; Khurana, I.; Di Iorio, J. R.; Li, H.; Albarracin Caballero, J. D.; Shih, A. J.; Anggara, T.; Delgass, W. N.; Miller, J. T.; et al. Catalysis in a Cage: Condition–Dependent Speciation and Dynamics of Exchanged Cu Cations in SSZ-13 Zeolites. *J. Am. Chem. Soc.* **2016**, *138* (18), 6028–6048.
- (48) Göltl, F.; Love, A. M.; Schuenzel, S. C.; Wolf, P.; Mavrikakis, M.; Hermans, I. Computational Description of Key Spectroscopic Features of Zeolite SSZ-13. *Phys. Chem. Chem. Phys.* **2019**, *21*, 19065–19075.
- (49) Göltl, F.; Love, A. M.; Hermans, I. Developing a Thermodynamic Model for the Interactions Between Water and Cu in the Zeolite SSZ-13. *J. Phys. Chem. C* **2017**, *121*, 6160–6169.
- (50) Di Iorio, J. R.; Gounder, R. Controlling the Isolation and Pairing of Aluminum in Chabazite Zeolites Using Mixtures of Organic and Inorganic Structure-Directing Agents. *Chem. Mater.* **2016**, *28*, 2236–2247.
- (51) Göltl, F.; Bulo, R. E.; Hafner, J.; Sautet, P. What Makes Copper-Exchanged SSZ-13 Zeolite Efficient at Cleaning Car Exhaust Gases? *J. Phys. Chem. Lett.* **2013**, *4*, 2244–2249.
- (52) Kulkarni, A. R.; Zhao, Z. J.; Siahrostami, S.; Nørskov, J. K.; Studt, F. Cation-Exchanged Zeolites for the Selective Oxidation of Methane to Methanol. *Catal. Sci. Technol.* 2018, 8 (1), 114–123.
- (53) Koishybay, A.; Shantz, D. F. Water Is the Oxygen Source for Methanol Produced in Partial Oxidation of Methane in a Flow Reactor over Cu-SSZ-13. J. Am. Chem. Soc. 2020, 142 (28), 11962–11966.
- (54) Olsbye, U.; Svelle, S.; Bjrgen, M.; Beato, P.; Janssens, T. V. W.; Joensen, F.; Bordiga, S.; Lillerud, K. P. Conversion of Methanol to Hydrocarbons: How Zeolite Cavity and Pore Size Controls Product Selectivity. *Angew. Chemie Int. Ed.* **2012**, *51* (24), 5810–5831.
- (55) Sushkevich, V. L.; Palagin, D.; van Bokhoven, J. A. The Effect of the Active-Site Structure on the Activity of Copper Mordenite in the Aerobic and Anaerobic Conversion of Methane into Methanol. *Angew. Chemie Int. Ed.* **2018**, *57* (29), 8906–8910.
- (56) Rosen, A. S.; Notestein, J. M.; Snurr, R. Q. Structure–Activity Relationships That Identify

- Metal–Organic Framework Catalysts for Methane Activation. *ACS Catal.* **2019**, *9*, 3576–3587.
- (57) Newton, M. A.; Knorpp, A. J.; Pinar, A. B.; Sushkevich, V. L.; Palagin, D.; Van Bokhoven, J. A. On the Mechanism Underlying the Direct Conversion of Methane to Methanol by Copper Hosted in Zeolites; Braiding Cu K-Edge XANES and Reactivity Studies. *J. Am. Chem. Soc.* **2018**, *140* (32), 10090–10093.
- (58) `Mahyuddin, M. H.; Tanaka, T.; Shiota, Y.; Staykov, A.; Yoshizawa, K. Methane Partial Oxidation over $[Cu2(\mu-O)]^{2+}$ and $[Cu3(\mu-O)3]^{2+}$ Active Species in Large-Pore Zeolites. *ACS Catal.* **2018**, *8* (2), 1500–1509.
- (59) Tsuchimura, Y.; Yoshida, H.; Machida, M.; Nishimura, S.; Takahashi, K.; Ohyama, J. Investigation of the Active-Site Structure of Cu-CHA Catalysts for the Direct Oxidation of Methane to Methanol Using In Situ UV-Vis Spectroscopy. *Energy and Fuels* **2023**, *37* (13), 9411–9418.

Table of Contents:



We modify activation conditions to stabilize different Cu-oxo and Cu-hydroxyl dimers in the zeolite SSZ-13. Subsequently we combine theory and experiment to investigate how the Cu site structure impacts the conversion of methane to methanol. Our results indicate that site stoichiometry controls methanol production in a stepwise conversion process.